

Selective Rollout: Mid-Trajectory Termination for Multi-Sample Agent RL

Zhiyuan Zhai

Fudan University
22110720067@m.fudan.edu.cn

Xin Wang

Fudan University
xwang11@fudan.edu.cn

Abstract

Group-relative RL training (GRPO) samples a small group of parallel rollouts for every training prompt and uses their within-group reward spread to compute per-trajectory advantages. In agentic environments each rollout is a long multi-turn dialogue with one LLM call per step, so this multi-sample multiplier dominates the total training cost. When every rollout of a prompt ends with the same reward, the group has zero reward variance and contributes no gradient, so the extra rollouts add no information; such groups are common in practice (typically around 40% of all groups), so the wasted-compute fraction is substantial rather than marginal. Existing methods filter such groups at the prompt level, either after their rollouts are paid for or before any rollout begins, but both decide without using information that becomes available during the rollout itself. We instead ask whether the in-group divergence between the partial trajectories at an intermediate step can already predict that the group will be zero-variance: when the parallel rollouts have already converged on the same action prefix, the group is on track to produce a single reward, and we can stop early. We propose a one-parameter gate that stops a group when the mean pairwise prefix edit distance between its partial action sequences falls below a threshold. On a 60-iteration on-policy GRPO run on ALFWorld with Qwen2.5-7B, averaged over four random seeds, the gated arm finishes **10.7%** faster in wall-clock (bootstrap 95% CI excludes 0) and shifts held-out success rate on 50 unseen tasks by **+2.5 pp**, with the held-out gain tracing to a measurable reduction in zero-advantage gradient-batch dilution. Code: <https://github.com/zhiyuanZhai20/selective-rollout>.

1 Introduction

Group-Relative Policy Optimization (GRPO [1, 2]) has become the dominant family of RL methods for fine-tuning language models on preference and outcome rewards [3], replacing the learned value baseline of PPO [4] with the empirical mean reward of a small group of parallel rollouts of the same prompt. The per-prompt cost of a GRPO iteration grows linearly with the number of rollouts in the group. In agentic environments such as ALFWorld [5], WebShop [6], or AgentBench [7] this multiplier matters more than usual: each rollout is a multi-turn dialogue, often 20–30 environment steps long with one LLM call per step, so a single rollout already takes minutes of wall-clock. Multiplying that by eight or sixteen rollouts per prompt makes the rollout phase the dominant cost in the entire training pipeline (~95% of wall-clock in our setup).

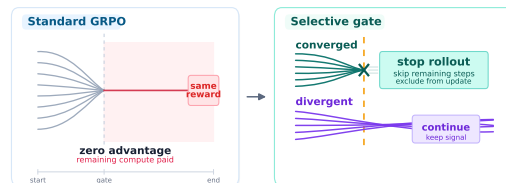


Figure 1: Selective rollout. Standard GRPO pays the full cost of converged groups (*left*); our gate stops them mid-rollout (*right*).

Not all of this compute is paying for new information. When every trajectory in a group ends with the same reward, the group has zero reward variance: the within-group normalisation sets every trajectory’s advantage to exactly zero, so the group contributes nothing to the policy gradient. Such groups are common in practice: with Qwen2.5-7B on ALFWorld, 39% of the offline groups we collect are zero-variance, and the rate hovers around 40% averaged across the 60 iterations of the on-policy training run in §4.3. Existing approaches recover this cost at the prompt level: DAPO [8] filters zero-variance groups out of the gradient batch *after* the rollouts have been paid for, while GRESO [9] predicts uninformative prompts *before* any rollout begins, using cross-epoch reward consistency on mathematical reasoning benchmarks. Both decide at the prompt level and leave the within-rollout compute untouched.

This paper asks: can we predict, partway through a group’s rollout, that the group is going to be zero-variance? If yes, we can stop the rollout early and recover the rest. The question makes sense only in an agentic setting. In a single-turn math problem there is no “partway through” to look at: the rollout is a single forward pass that either finishes or does not. In an agent rollout, by contrast, the group’s trajectories interact with the environment over many steps, and at any intermediate step we can compare the partial trajectories produced so far. Our hypothesis is that when these partial trajectories have already converged on a single action sequence at the chosen intermediate step, the group is on track to be zero-variance: the policy has effectively committed to one behaviour, and the remaining steps will only confirm that commitment. Conversely, divergent prefixes signal a group that is still meaningfully exploring and worth letting run.

We test this hypothesis on 100 ALFWorld groups with group size eight and find that a single threshold on the mean pairwise prefix-edit distance suffices. The same gate then drops into a 60-iteration on-policy GRPO training loop, where it produces a measurable wall-clock saving with no degradation (and a small directional improvement) on held-out evaluation. We also give a quantitative account of *why* the gated policy learns at least as well: removing zero-variance groups raises the effective per-step gradient signal-to-noise by exactly the amount predicted by a simple dilution argument on the GRPO loss.

Contributions.

- **A one-parameter mid-rollout gate** based on in-group prefix-edit divergence at step K . On $N = 100$ ALFWorld groups with $G = 8$, the gate recovers **14.0%** of rollout step-tokens at offline precision 0.81 (**11.3%** losslessly) while preserving **96.7%** of the GRPO advantage L^2 -norm.
- **End-to-end on-policy validation.** Across $n = 4$ seeds of a 60-iteration on-policy GRPO training run, the gated arm finishes **10.7%** faster (bootstrap 95% CI excludes 0) and shifts held-out success on 50 unseen tasks by **+2.5 pp**.
- **Mechanistic explanation of the held-out gain.** The gate lowers the gradient-batch zero-advantage fraction from $\sim 40\%$ to $\sim 28\%$, raising the measured gradient L^2 -norm by **1.16×**, in quantitative agreement with the predicted dilution effect.

We defer the full related-work discussion to App. A.

2 Preliminaries

2.1 GRPO

Let π_θ be a language-model policy and \mathcal{D} a distribution over agent prompts. For prompt $x \sim \mathcal{D}$, GRPO [1] samples a group of G rollouts $\{\tau_1, \dots, \tau_G\}$ from π_θ , each a sequence of (observation, action, reward) triples up to horizon T_{\max} . Let $r_i = R(\tau_i)$ be the terminal reward. The group-relative advantage is

$$A_i = \frac{r_i - \bar{r}}{\sigma_r + \varepsilon}, \quad \bar{r} = \frac{1}{G} \sum_j r_j, \quad \sigma_r = \sqrt{\frac{1}{G} \sum_j (r_j - \bar{r})^2}. \quad (1)$$

Intuitively, A_i is the within-group z -score of r_i : it is positive when trajectory i scored above the group mean and the policy should be pushed *toward* reproducing it, negative when below the mean (push away), and zero when $r_i = \bar{r}$. The REINFORCE-style [10] policy-gradient loss is $\mathcal{L}(\theta) = -\frac{1}{N} \sum_i A_i \log p_\theta(\tau_i)$, averaged over all N trajectories in the gradient batch (agent-specific teacher-forcing in App. C.2).

A group is *zero-variance* when σ_r is zero, that is, when all G trajectories in the group end with the same reward. For such a group the advantage A_i is zero for every i , so the group contributes nothing to the policy gradient.

This zero contribution causes a second, more subtle effect that will be important later. The policy-gradient loss above is the *mean* over all N trajectories in the batch, so it divides by N . A trajectory whose advantage is zero does not add to the numerator of this mean, but it still occupies one of the N slots in the denominator. The result is that the gradient contributed by the trajectories with non-zero advantage is shrunk by a factor equal to the fraction of non-zero-advantage trajectories in the batch. If half the trajectories in a batch have advantage zero, the effective gradient is half what it would be on a batch of only non-zero-advantage trajectories. We return to this effect in §4.4.

2.2 Compute decomposition in agent RL

We measure compute in two ways throughout the paper. **Wall-clock** is real elapsed seconds on the GPU, and **step-tokens** is the total number of action tokens the policy emits across all rollouts; an implementation-independent measure of generation cost. Each GRPO iteration in our setting consists of three phases:

- **Rollout (sampling)**. The policy generates the G trajectories one token at a time. For ALFWorld with $T_{\max} = 30$ and $G = 8$ this is on the order of 240 generation calls per prompt, with no gradient computation. In our on-policy training runs this phase consumes $\sim 95\%$ of total wall-clock.
- **Advantage computation**: Eq. 1. Negligible cost.
- **Training (gradient update)**. For each sampled trajectory the trainer evaluates the policy on the full token sequence to recover the per-action log-probabilities $\log p_\theta(a_t | \text{prefix})$, then computes the policy-gradient loss and backpropagates it to update the LoRA parameters. The cost per token is roughly $50\times$ larger than during sampling (because gradients require activation memory and quadratic-in-length attention), but it operates only on the trajectories in the batch, not on every rollout that was sampled.

A zero-variance group wastes all three phases: it pays the full rollout cost, computes a zero advantage, and (unless filtered) contributes a zero loss with the full gradient-update cost. The gate we develop next eliminates the post- K tail of the rollout cost in addition to the training cost.

3 Selective-rollout gate

3.1 Setup

For the predictive analysis in this section we use a fixed corpus of $N = 100$ rollouts. Prompts are drawn uniformly at random from the ALFWorld [5] `valid_seen` split and cover all six task types in proportions $\{\text{pick_and_place_simple}, \text{pick_two_obj}, \text{pick_clean}, \text{pick_heat}, \text{pick_cool}, \text{look_at_obj}\} = \{24, 20, 18, 11, 19, 8\}$. The policy is Qwen2.5-7B-Instruct [11], sampled at temperature $T = 0.7$ with group size $G = 8$ and rollout horizon $T_{\max} = 30$. Across the 100 groups we observe 25 all-fail, 61 mixed, and 14 all-succeed groups (a 39% zero-variance rate). All code, raw rollouts, divergence metrics, gate-sweep results, and training logs are released as supplementary material.

3.2 Mid-rollout signals and the gate

Let $a_{i,t}$ be the action emitted by trajectory i at environment step t . At an intermediate step $K \leq T_{\max}$ we want a scalar measure of how much the G partial trajectories disagree with each other so far. The signal we use throughout the paper is the **mean pairwise prefix edit distance** $d_K \in [0, 1]$: for each pair (i, j) we take the Levenshtein [12] edit distance between the action sequences $a_{i,1:K}$ and $a_{j,1:K}$, normalise by the longer of the two lengths, and average over all $\binom{G}{2}$ pairs. $d_K = 0$ means all G prefixes are identical and $d_K = 1$ means no two trajectories share any actions in their first K steps. We considered six other in-group divergence signals (action-bigram Jaccard, unique-prefix ratio, unique-action ratio, action entropy, observation-unique ratio, and termination fraction) and pick d_K because it is among the strongest predictive signals at $K \in \{10, 15\}$ (§3.3, Fig. 2) and is the most directly interpretable. Full definitions and the side-by-side comparison are in App. B. To label

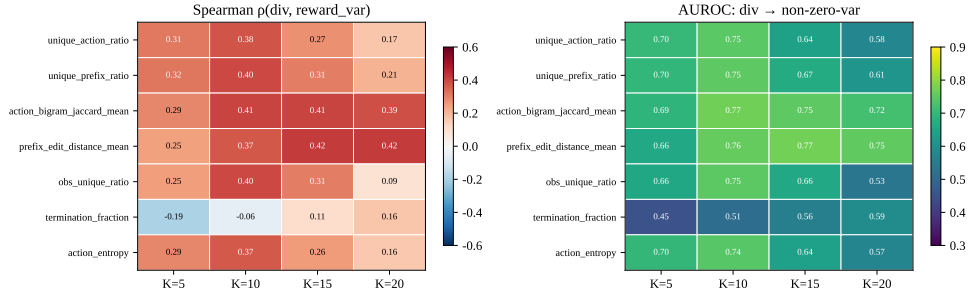


Figure 2: Spearman ρ (left) and AUROC for non-zero-variance classification (right) for each (metric, K) cell, $N = 100$, $G = 8$. The single-axis signal peaks at $K \in \{10, 15\}$ and degrades at the extremes.

groups in the predictive analysis below we use the binary label $\mathbf{1}[\sigma_r = 0]$ and the three-way label $\ell \in \{\text{all_fail}, \text{mixed}, \text{all_succeed}\}$, both computed only after the rollout finishes.

The gate. We propose a one-parameter gate that is evaluated at step K and decides whether to terminate the group:

$$\text{CUT}_{K,d_L}(\tau_{1:G}) = \left[d_K < d_L \right]. \quad (2)$$

The gate fires when the G partial trajectories have already converged on the same action prefix at step K . This happens in two situations: either the policy is confident about the task and all G rollouts are heading toward the same successful behaviour, or the policy has gotten stuck in an early loop and all G rollouts are repeating the same failing actions. When the gate fires, the group is removed from the GRPO update entirely: any trajectories in the group that are still running are stopped at step K , and the entire group is dropped from the gradient batch (i.e. none of its trajectories enter \mathcal{L} in Eq. 1). The compute saving is therefore twofold: the post- K rollout cost ($T_{\max} - K$ generation steps per trajectory in the group) and the training-step cost (forward and backward pass over those trajectories). Implementation details for the rollout-loop integration are in App. C.1.

3.3 Mid-rollout divergence correlates with reward variance

For each of the seven divergence measures defined in §3.2 and each evaluation step $K \in \{5, 10, 15, 20\}$, we ask two questions about the 100 groups in our buffer. First, how strongly does the divergence value at step K correlate (in rank order) with the final reward variance of the group? We measure this with Spearman’s rank correlation ρ . Second, how well does the same divergence value distinguish zero-variance groups from non-zero-variance groups when treated as a binary classifier score? We measure this with AUROC. The full 7×4 heat map is shown in Fig. 2, with the underlying table in App. E.3.

The signal is strongest at $K \in \{10, 15\}$. For prefix edit distance (d_K) at $K = 15$, ρ reaches 0.42 ($p = 1.4 \times 10^{-5}$) and AUROC reaches 0.77. The other six divergence measures show qualitatively similar patterns: all of them rise into the same regime around $K = 10$ – 15 and fall off at the extremes ($K = 5$ is too early, $K = 20$ leaves too few steps to recover). We choose d_K for the gate because it is the most consistent of the seven across K values and because it has a direct interpretation as an average pairwise edit distance. Breaking the same d_{10} signal down by ALFWORLD task type shows that the signal generalises across tasks but unevenly. The median per-type AUROC is 0.76, with values ranging from 0.48 to 1.00 across the six task types. If we are allowed to tune the metric and the evaluation step K separately for each task type, the worst case rises to AUROC 0.71 and the median to 0.86 (App. E.5).

3.4 Where the signal lives: $d_{K=10}$ stratified by group label

Figure 3 explains how the cut region splits across the three group labels. Both all-succeed and all-fail groups have a sub-population at low d_K , and the gate at $d_L = 0.12$ catches both: of the 17 true-positive cuts, 7 are from the 14 all-succeed groups and 10 are from the 25 all-fail groups. The all-succeed cluster (green) is more tightly concentrated at low d_K and the gate catches half of it (7/14); the all-fail cluster (red) has a heavier right tail that overlaps with the mixed cluster, so the

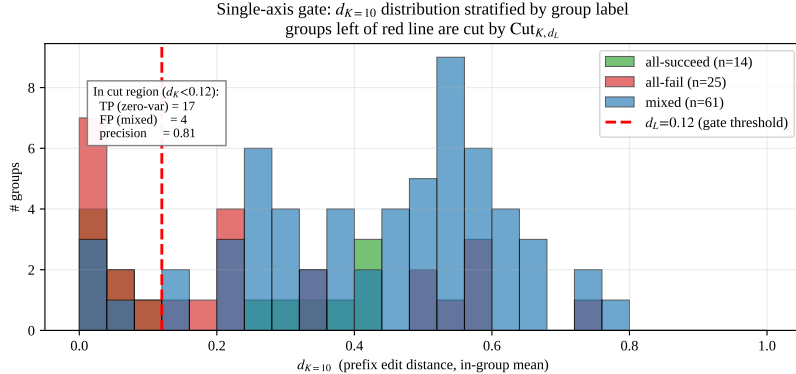


Figure 3: Distribution of $d_{K=10}$ on the $N = 100$ buffer, coloured by the group’s final outcome (determined only after the full rollout completes, by inspecting the multiset of G final rewards). At $d_L = 0.12$ (red dashed line) the gate catches 7/14 all-succeed and 10/25 all-fail groups (the 17 true positives) plus 4/61 mixed groups (false positives). The high- d_K tail of the all-fail cluster overlaps with the mixed cluster, so raising d_L would break the precision floor (§5).

Table 1: Single-axis gate CUT_{K,d_L} at $K = 10$ on $N = 100$ groups (39 zero-variance) for varying threshold d_L . Columns: **cut** = total groups the gate fires on (= TP+FP), **TP** = correctly cut zero-variance groups, **FP** = mistakenly cut non-zero-variance groups, **prec.** = TP/cut, **recall** = TP/39, **safe** = the lossless step-token recovery from TP cuts alone, $\text{TP} \cdot (T_{\max} - K) / (N \cdot T_{\max})$ (TPs have advantage exactly 0, so dropping them removes no gradient signal), **raw** = the total step-token recovery from all cuts, $\text{cut} \cdot (T_{\max} - K) / (N \cdot T_{\max})$ (this is the quantity wall-clock actually drops by; the difference raw – safe is the rollout cost of FP cuts and corresponds to a small L^2 -norm signal loss). Operating points are subject to a precision floor of ≥ 0.80 to bound false-positive cost (derivation in App. C.5).

d_L	cut	TP	FP	prec.	recall	safe (%)	raw (%)	note
0.05	9	9	0	1.00	0.23	6.0	6.0	most conservative
0.08	14	13	1	0.93	0.33	8.7	9.3	
0.10	20	16	4	0.80	0.41	10.7	13.3	at floor
0.12	21	17	4	0.81	0.44	11.3	14.0	chosen, used in all online runs
0.14	24	18	6	0.75	0.46	12.0	16.0	below floor
0.18	25	19	6	0.76	0.49	12.7	16.7	below floor

gate only reaches its low- d_K end (10/25). The mixed cluster (the 61 groups with both wins and losses) has a right tail at higher d_K that the gate correctly leaves alone, and a left tail at lower d_K that produces the four false positives we discuss in the ablation below. Raising d_L to reach the remaining ~ 15 high- d_K all-fail groups would pull in many more mixed groups as false positives and break the precision floor.

3.5 Choosing K and d_L , and the savings–signal tradeoff

Table 1 sweeps d_L at $K = 10$. We pick $d_L = 0.12$, which sits at the precision-floor boundary and is used in all online experiments (§4): it cuts 21 groups (17 TPs, 4 FPs), recovering 14.0% of step-tokens raw, of which 11.3% is lossless (TPs have advantage 0) and 2.7% is the FP cost. The raw 14.0% matches the wall-clock saving Tier 1 (§4.1) measures online (-13.25% , within rounding). $K = 10$ is the sweet spot: $K = 5$ admits no operating point above the floor; $K \geq 15$ leaves too few post- K steps to recover. The 4 FPs all share one failure mode (a fixed drawer-by-drawer search prefix on `pick_and_place_simple`), pointing at a generic limitation of action-prefix signals (App. E.4).

Savings vs gradient signal preserved. TP cuts are lossless because their advantages are 0; only FPs cost signal. Computing $\|A_{\text{kept}}\|_2 / \|A_{\text{full}}\|_2$ on the buffer at ($K = 10, d_L = 0.12$) gives 96.7%. The gate trades the 2.7% FP rollout saving for a 3.3% L^2 -norm loss, an order-of-magnitude favourable

Table 2: Experimental setup across the three integration tiers. In Tier 1 the same 100 tasks are run twice (baseline and gated) with matched random seeds. In Tier 3 the trained policy weights are loaded back into the inference engine after every iteration.

	Tier 1: Rollout	Tier 2: Off-policy	Tier 3: On-policy
purpose	rollout-time saving	training-time saving	full end-to-end loop
prompt budget	100 tasks ($\times 2$ arms)	100 tasks (replay buffer)	10 prompts/iter \times 60 iters
gradient updates	none	20 LoRA steps	60 iterations
trajectory source	current θ	θ_0 (frozen)	current θ_t
held-out eval	—	—	50 tasks, every 10 iters

Common to all tiers
 Base model: Qwen2.5-7B-Instruct [11]. Environment: ALFWorld [5] valid_seen, six task types, $T_{\max} = 30$, sample $T = 0.7$.
 Group size $G = 8$ unless stated. Gate $(K, d_L) = (10, 0.12)$. Hardware: NVIDIA RTX 6000 Ada (48 GB).
 Per-tier LoRA, optimiser, and random seed(s) are listed in App. C.4, Table 6.

balance. At the more-conservative $d_L = 0.08$ (one FP, precision 0.93), preservation rises to 99.0% but raw savings drop to 9.3% (App. E.2).

4 Online integration: three-tier validation

We validate the gate at three progressively more realistic integration points (Table 2): **Tier 1** measures the rollout-phase wall-clock saving alone, with no policy updates, a clean A/B test of the gate’s effect on rollout time. **Tier 2** adds 20 GRPO training steps over a fixed rollout buffer to isolate the training-phase saving (the policy does not change between rollouts). **Tier 3** adds the full closed loop (60 on-policy GRPO iterations in which the policy is updated after each group of rollouts and the next iteration’s rollouts use the updated policy) and adds held-out evaluation against 50 unseen tasks.

The Tier-3 held-out split of 50 valid_seen tasks is disjoint by task instance from the 10 prompts used per training iteration.

4.1 Tier 1 — Rollout-only A/B

We compare two ways of generating rollouts on the same 100 ALFWorld prompts, in a fresh A/B re-run rather than a re-analysis of the §3.1 offline buffer. The **baseline** run rolls each task out for the full 30 environment steps, sampling $G = 8$ trajectories per task. The **gated** run does the same, but at step 10 it pauses each group, computes the divergence d_{10} between its eight partial trajectories, and stops the group if $d_{10} < 0.12$. The remaining 20 steps are then skipped for that group. Both runs use the same random seed for sampling, so the first 10 steps are identical between arms; the only difference is whether post- K steps are generated.

We measure the total wall-clock spent generating rollouts in each run. The gate stops 20 of the 100 groups at step 10 (21 in the offline ablation; Table 1, the 1-group difference is LLM sampling non-determinism across the two re-runs). To check how many of these 20 groups were the “right” ones to stop (meaning their full rollout would have ended zero-variance, so stopping at step 10 lost no information), we compare against the baseline run, which provides the ground-truth final reward distribution for each group. 19 of the 20 groups the gate cut turn out to be zero-variance (empirical precision 0.95). Total rollout wall-clock drops by **13.25%**; resampling the 100 tasks with replacement 1,000 times gives a percentile bootstrap [13] 95% confidence interval on the saving of [7.55, 19.12]%, which excludes zero (Table 3). The Tier 1 wall-clock CI uses task bootstrap; multi-seed Tier-3 numbers (Table 5) report sample std across $n = 4$ seeds.

4.2 Tier 2 — Off-policy GRPO training A/B

Tier 1 measured only the time spent generating rollouts. We next check that the gate also reduces the cost of the training step itself. We re-use the same 100 ALFWorld groups (each is a prompt together with its $G = 8$ rolled-out trajectories and their rewards) as a fixed buffer, and run a 20-step GRPO training loop over this buffer. At each of the 20 training steps we sample 4 groups from the buffer, compute the group-relative advantages from Eq. 1, and take one AdamW [14] update on the LoRA parameters of Qwen2.5-7B.

In the gated arm we apply the same gate before forming the training batch. The gate condition uses the d_{10} value already recorded in the buffer for each group; a group whose $d_{10} < 0.12$ is dropped

Table 3: **Tier 1.** Rollout-phase A/B on $N = 100$ ALFWorld tasks; the same task set is rolled out twice, once without the gate and once with it, using the same random seeds so the only difference is gate-induced early termination. $G = 8$ trajectories per task, gate $\text{CUT}_{K=10, d_L=0.12}$. Of the 20 groups cut by the gate in the gated arm, 19 turned out to be zero-variance once the matched baseline arm completed (empirical precision 0.95). The bootstrap 95% confidence interval on the wall-clock saving (resampling tasks 1,000 times with replacement) is [7.55, 19.12]%

	baseline	gated	Δ
total wall-clock (s)	2,678.6	2,323.9	−13.25%
mean per-task (s)	26.8	23.2	−13.25%
groups cut (of 100)	0	20	+20

Table 4: **Tier 2.** Off-policy GRPO training A/B on Qwen2.5-7B + LoRA, 20 steps, 4 groups/step, $G = 8$ trajectories per group from a frozen $N = 100$ buffer.

	baseline	gated	Δ
total step wall-clock (s)	496.0	336.3	−32.2%
total train items	2,560	1,984	−22.5%
groups cut (out of 80)	0	18	cut rate 22.5%
gradient L^2 -norm mean	0.086	0.098	+14.0%

from this training step’s batch, and the loss is averaged over the remaining trajectories. Because the buffer is fixed and the policy is not used to generate new rollouts between training steps, the only difference between the two arms is whether or not the cut groups enter each step’s gradient batch. This isolates the training-side effect of the gate from any rollout-generation differences.

Across the 20 training steps and 4 groups per step, the gate drops 18 of the 80 groups it sees, which matches the prediction from the offline analysis. The mean per-step gradient L^2 -norm rises by 14% in the gated arm (Table 4). This is the dilution effect we described above made concrete: the dropped groups had advantages exactly zero, so removing them does not change the numerator of the gradient mean, but it shrinks the denominator, and the remaining trajectories’ gradient becomes proportionally larger. We give the full derivation in §4.4. End-to-end training wall-clock drops by 32.2%, because each dropped group also avoids its forward and backward pass through the model. The per-step trace is in App. E.7.

4.3 Tier 3 — On-policy GRPO training A/B with held-out eval

Tier 3 is the full closed-loop on-policy GRPO run: at each of 60 iterations we draw 10 ALFWorld prompts, sample $G = 8$ trajectories per prompt (the gate is active in the gated arm and inactive in the baseline arm), compute group-relative advantages (Eq. 1), and take one AdamW update on the LoRA parameters of Qwen2.5-7B; updated weights are hot-swapped into the inference engine before the next iteration (App. C.3). Every 10 iterations both arms are evaluated greedily on 50 unseen `valid_seen` tasks. We repeat the experiment with 4 random seeds, with each baseline run paired to a gated run sharing the same seed so the only difference is the gate (per-iter trace in App. E.8).

The wall-clock saving (Fig. 4 top-right) is consistent across seeds: every seed lies in [8.95, 14.16]% and the mean is 10.7% with a bootstrap 95% CI that excludes zero. The gradient L^2 -norm rises by 1.16 \times in the gated arm, in quantitative agreement with the dilution prediction of §4.4. Held-out success (Fig. 4 top-left): both arms start from the same pre-trained checkpoint at iter 0, so the two iter-0 points coincide per-seed (their across-seed std of 3.0 pp reflects only the seeded 50-task held-out subset); the curves diverge with training and reach 41.5% (baseline) vs. 44.0% (gated) at iter 60, a +2.5 pp gap (per-seed +4, +6, +2, −2 pp). The shift is directionally favourable but not statistically significant at $n = 4$. The bottom-right panel of Fig. 4 validates the core assumption: at each iteration the gate fires on roughly the same number of groups that the matched baseline arm later finds to be zero-variance, indicating the gate selects the intended targets. The training-reward panel (bottom-left) uses a corrected mean: cut groups are excluded from the gated curve because they are stopped at $K = 10$, before most ALFWorld successes arrive (typically between steps 15 and 25), and including their truncated reward of 0 would unfairly bias the gated mean downward; after this correction the gated training reward sits slightly above baseline, consistent with the 1.16 \times gradient amplification we explain in §4.4.

Table 5: **Tier 3.** On-policy GRPO training A/B with the gate ($K = 10$, $d_L = 0.12$) on Qwen2.5-7B + LoRA, 60 iterations, 10 prompts/iter, $G = 8$, averaged over $n = 4$ seeds ($\{7, 13, 23, 42\}$). Held-out eval is greedy on 50 valid_seen ALFWorld tasks, never seen during training. Per-seed pre-training eval values are 38, 44, 38, 38% (mean $39.5 \pm 3.0\%$); per-seed held-out delta at iter 60 is +4, +6, -2, +2 pp. Standard deviations across the 4 seeds: total wall-clock $\pm 187 / \pm 534$ s; gradient $L^2 \pm 0.001 / \pm 0.008$; held-out eval $\pm 4.4 / \pm 7.1$ pp.

	baseline	gated	Δ
total wall-clock (s)	$17,393 \pm 187$	$15,527 \pm 534$	$-10.7 \pm 2.4\%$
groups cut by gate (of 600)	0	106 ± 18	+106
gradient L^2 -norm	0.125 ± 0.001	0.145 ± 0.008	$1.16 \pm 0.07 \times$
held-out eval, iter 0 (pre-training)	$39.5 \pm 3.0\%$	$39.5 \pm 3.0\%$	0
held-out eval, iter 60	$41.5 \pm 4.4\%$	$44.0 \pm 7.1\%$	$+2.5 \pm 3.4$ pp

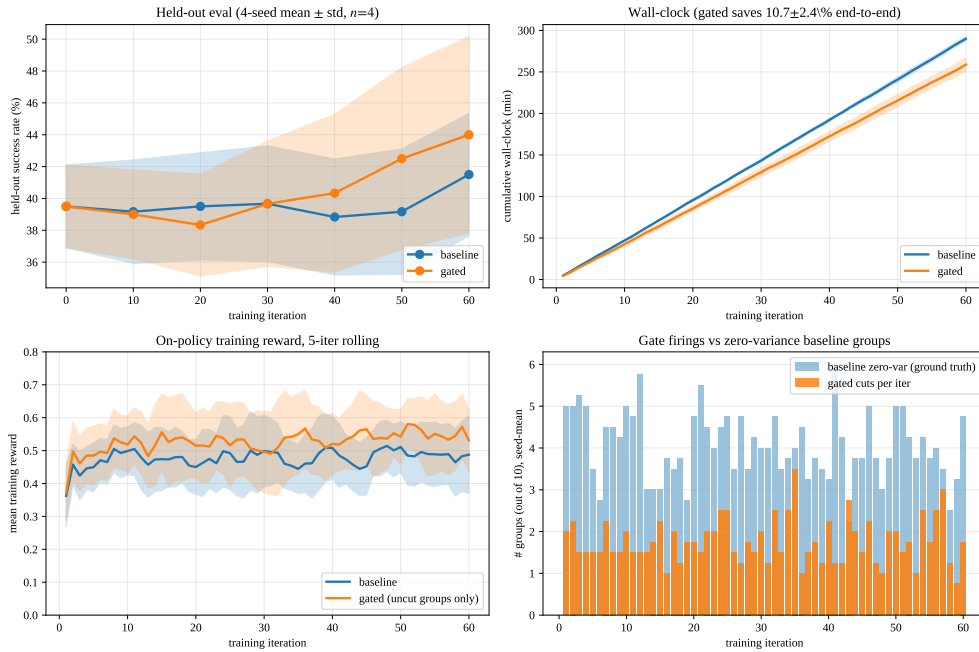


Figure 4: On-policy GRPO A/B on Qwen2.5-7B + LoRA, gate $CUT_{K=10, d_L=0.12}$, averaged over $n = 4$ seeds $\{7, 13, 23, 42\}$; bands are ± 1 std across seeds. *Top-left*: held-out success on 50 unseen tasks (every 10 iter). *Top-right*: cumulative wall-clock; gated runs 10.7% shorter at iter 60. *Bottom-left*: per-iter mean training reward (5-iter rolling), gated averaged over uncut groups only. *Bottom-right*: per-iter gate cut count (orange) vs. baseline zero-variance count (blue); the gate fires predominantly on the same groups the baseline arm later finds to be zero-variance.

Taken together, the gate is robustly compute-saving, at worst neutral on policy quality, with a directionally positive but not statistically significant trend toward better held-out success.

4.4 Why on-policy gated learns better: dilution mechanics

The GRPO advantage of a trajectory is its reward z -score within its group (Eq. 1). When the group is zero-variance, every trajectory in the group has advantage exactly zero, so each one contributes nothing to the gradient numerator. The loss the trainer minimises, however, is the mean over *all* trajectories in the batch, so each zero-advantage trajectory still occupies one slot in the denominator. The result is that the gradient contributed by the remaining non-zero-advantage trajectories is divided by a denominator that is larger than necessary, and the effective update is shrunk.

We can quantify this effect from the per-iteration training logs. In the un-gated baseline run, the mean fraction of trajectories per batch that have advantage exactly zero is about 40% (zero-variance groups produce eight zero-advantage trajectories each, so the rate tracks the zero-variance group rate).

The gate removes about 18% of groups before they enter the batch, which brings the zero-advantage fraction down to about 28%. The fraction of trajectories that contribute to the gradient therefore rises from about $1 - 0.40 = 0.60$ to about $1 - 0.28 = 0.72$. If the contributing trajectories’ gradients are otherwise of comparable magnitude in the two arms, the gradient norm in the gated arm should be larger than the baseline gradient norm by a factor of $0.72/0.60 \approx 1.20$.

We measure the gradient L^2 -norm in both arms over the 60 iterations and across the 4 seeds. The gated arm’s gradient norm is on average 1.16 ± 0.07 times the baseline value (per-seed 1.10, 1.10, 1.20, 1.23; Table 5), close to the predicted 1.20; the small gap suggests non-zero-advantage groups surviving the gate have slightly smaller gradient magnitudes than the average non-zero-advantage group, an effect a pure dilution argument does not capture. Both arms use the same nominal learning rate, but the gated arm takes a per-step parameter update that is roughly 16% larger in L^2 norm, which we believe is the source of the directional improvement on held-out success. Extended derivation, the over-training mechanism evolution, and a token-level dilution measurement are in App. D.1, E.12, E.13.

The appendix collects the supporting material: $G = 8$ vs $G = 16$ robustness (App. E.6), calibration against random-cut and oracle gates (App. E.1), strong-baseline comparisons (App. E.11), hyperparameters and hardware (App. C.4, C.6), and prompt templates (App. F).

5 Discussion

Relation to prompt-level filters. DAPO [8] drops zero-variance groups from the gradient batch *after* their rollouts have been generated, so it saves the training-step cost but not the rollout cost. GRESO [9] predicts zero-variance prompts *before* any rollout begins, using cross-epoch reward consistency on math benchmarks; it has no way to use information that becomes available *during* a rollout. Our gate is orthogonal to both: it operates mid-rollout, before the group’s reward variance is known, using only the partial trajectories observed up to step K . The two filters compose naturally: our gate cuts the low- d_K end of both convergent-success and convergent-failure groups mid-rollout to save the post- K rollout cost, while DAPO cleans up the high- d_K tail of convergent-failure groups (which our prefix-divergence signal cannot reach without breaking the precision floor; §3.5) by dropping any surviving zero-variance groups from the gradient batch. We treat OURS+DAPO as the recommended production combination (App. E.11, Table 12).

Practical use. The gate adds no new training-time hyperparameters beyond the single threshold d_L , which we tuned once on the offline buffer (§3.5) and reused without retuning across all three online integration tiers. Runtime overhead is negligible: computing d_K on a group of G partial action sequences of length K amounts to at most $\binom{G}{2}$ pairwise Levenshtein distances on short token strings, which costs microseconds per group and is dominated by the rollout itself. The gate composes naturally with prompt-level filtering (DAPO [8]) and with parameter-efficient fine-tuning (LoRA [49]) that we use in our online runs.

Limitations. The gate catches both convergent-success and convergent-failure groups (Fig. 3: 7/14 all-succeed and 10/25 all-fail at $d_L = 0.12$), but it cannot reach the high- d_K tail of the all-fail cluster, where the early-action distributions overlap with mixed-outcome groups. A two-clause OR-rule adding a termination-fraction condition does not clear the 0.80 precision floor either, so the limitation is structural (App. E.9, E.10). Other limitations: the on-policy run uses $n = 4$ seeds, so the held-out shift is directional but not significant; model and environment are fixed (Qwen2.5-7B + ALFWorld), so cross-setting transfer is unverified; and K is a fixed hyperparameter rather than chosen adaptively.

Conclusion. A single-threshold mid-rollout gate on in-group prefix-edit divergence recovers a measurable fraction of GRPO rollout compute in agent RL without degrading (and modestly improving) held-out policy quality. The held-out improvement is mechanistic: removing zero-advantage groups raises the per-step gradient signal-to-noise by the dilution-predicted amount, so the gated arm takes effectively larger updates at the same nominal learning rate. Adaptive K and complementary signals (e.g., environment-side progress proxies) for the high- d_K tail of zero-variance groups our prefix-divergence signal misses are natural follow-ups.

References

- [1] Zhihong Shao, Peiyi Wang, Qihao Zhu, Runxin Xu, Junxiao Song, Xiao Bi, Haowei Zhang, Mingchuan Zhang, Y.K. Li, Y. Wu, and Daya Guo. Deepseekmath: Pushing the limits of mathematical reasoning in open language models. *arXiv preprint arXiv:2402.03300*, 2024.
- [2] DeepSeek-AI, Daya Guo, Dejian Yang, Haowei Zhang, Junxiao Song, Ruoyu Zhang, Runxin Xu, Qihao Zhu, Shirong Ma, Peiyi Wang, Xiao Bi, et al. Deepseek-r1: Incentivizing reasoning capability in llms via reinforcement learning. *arXiv preprint arXiv:2501.12948*, 2025.
- [3] Long Ouyang, Jeffrey Wu, Xu Jiang, Diogo Almeida, Carroll Wainwright, Pamela Mishkin, Chong Zhang, Sandhini Agarwal, Katarina Slama, Alex Ray, et al. Training language models to follow instructions with human feedback. In *Advances in Neural Information Processing Systems*, 2022.
- [4] John Schulman, Filip Wolski, Prafulla Dhariwal, Alec Radford, and Oleg Klimov. Proximal policy optimization algorithms. *arXiv preprint arXiv:1707.06347*, 2017.
- [5] Mohit Shridhar, Kingdi Yuan, Marc-Alexandre Côté, Yonatan Bisk, Adam Trischler, and Matthew Hausknecht. Alfworld: Aligning text and embodied environments for interactive learning. In *International Conference on Learning Representations (ICLR)*, 2021.
- [6] Shunyu Yao, Howard Chen, John Yang, and Karthik Narasimhan. Webshop: Towards scalable real-world web interaction with grounded language agents. In *Advances in Neural Information Processing Systems*, 2022.
- [7] Xiao Liu, Hao Yu, Hanchen Zhang, Yifan Xu, Xuanyu Lei, Hanyu Lai, Yu Gu, Hangliang Ding, Kaiwen Men, Kejuan Yang, et al. Agentbench: Evaluating llms as agents. In *International Conference on Learning Representations (ICLR)*, 2024.
- [8] Qiying Yu, Zheng Zhang, Ruofei Zhu, Yufeng Yuan, Xiaochen Zuo, Yu Yue, Weinan Dai, Tiantian Fan, Gaohong Liu, Lingjun Liu, et al. Dapo: An open-source llm reinforcement learning system at scale. *arXiv preprint arXiv:2503.14476*, 2025.
- [9] Haizhong Zheng, Yang Zhou, Brian R. Bartoldson, Bhavya Kailkhura, Fan Lai, Jiawei Zhao, and Beidi Chen. Act only when it pays: Efficient reinforcement learning for llm reasoning via selective rollouts. *arXiv preprint arXiv:2506.02177*, 2025.
- [10] Ronald J. Williams. Simple statistical gradient-following algorithms for connectionist reinforcement learning. *Machine learning*, 8:229–256, 1992.
- [11] Qwen Team. Qwen2.5 technical report. *arXiv preprint arXiv:2412.15115*, 2024.
- [12] Vladimir I. Levenshtein. Binary codes capable of correcting deletions, insertions, and reversals. *Soviet Physics Doklady*, 10(8):707–710, 1966.
- [13] Bradley Efron. Bootstrap methods: Another look at the jackknife. *The Annals of Statistics*, 7(1):1–26, 1979.
- [14] Ilya Loshchilov and Frank Hutter. Decoupled weight decay regularization. In *International Conference on Learning Representations (ICLR)*, 2019.
- [15] John Schulman, Sergey Levine, Pieter Abbeel, Michael Jordan, and Philipp Moritz. Trust region policy optimization. In *International Conference on Machine Learning (ICML)*, pages 1889–1897, 2015.
- [16] Richard S. Sutton and Andrew G. Barto. *Reinforcement learning: An introduction*. MIT Press, second edition, 2018.
- [17] Arash Ahmadian, Chris Cremer, Matthias Gallé, Marzieh Fadaee, Julia Kreutzer, Olivier Pietquin, Ahmet Üstün, and Sara Hooker. Back to basics: Revisiting reinforce-style optimization for learning from human feedback in llms. In *Proceedings of the 62nd Annual Meeting of the Association for Computational Linguistics (ACL)*, pages 12248–12267, 2024.
- [18] Ziniu Li, Tian Xu, Yushun Zhang, Zhihang Lin, Yang Yu, Ruoyu Sun, and Zhi-Quan Luo. Remax: A simple, effective, and efficient reinforcement learning method for aligning large language models. In *International Conference on Machine Learning (ICML)*, 2024.

- [19] Zichen Liu, Changyu Chen, Wenjun Li, Penghui Qi, Tianyu Pang, Chao Du, Wee Sun Lee, and Min Lin. Understanding r1-zero-like training: A critical perspective. In *Conference on Language Modeling (COLM)*, 2025.
- [20] Jian Hu. Reinforce++: A simple and efficient approach for aligning large language models. *arXiv preprint arXiv:2501.03262*, 2025.
- [21] Paul F. Christiano, Jan Leike, Tom B. Brown, Miljan Martic, Shane Legg, and Dario Amodei. Deep reinforcement learning from human preferences. In *Advances in Neural Information Processing Systems*, 2017.
- [22] Nisan Stiennon, Long Ouyang, Jeffrey Wu, Daniel M. Ziegler, Ryan Lowe, Chelsea Voss, Alec Radford, Dario Amodei, and Paul F. Christiano. Learning to summarize with human feedback. In *Advances in Neural Information Processing Systems*, 2020.
- [23] Rafael Rafailov, Archit Sharma, Eric Mitchell, Stefano Ermon, Christopher D. Manning, and Chelsea Finn. Direct preference optimization: Your language model is secretly a reward model. In *Advances in Neural Information Processing Systems*, 2023.
- [24] Yuntao Bai, Saurav Kadavath, Sandipan Kundu, Amanda Askell, John Kernion, Andy Jones, Anna Chen, Anna Goldie, Azalia Mirhoseini, Cameron McKinnon, et al. Constitutional ai: Harmlessness from ai feedback. *arXiv preprint arXiv:2212.08073*, 2022.
- [25] Harrison Lee, Samrat Phatale, Hassan Mansoor, Thomas Mesnard, Johan Ferret, Kellie Lu, Colton Bishop, Ethan Hall, Victor Carbune, Abhinav Rastogi, et al. Rlaif vs. rlhf: Scaling reinforcement learning from human feedback with ai feedback. In *International Conference on Machine Learning (ICML)*, 2024.
- [26] Yoshua Bengio, Jérôme Louradour, Ronan Collobert, and Jason Weston. Curriculum learning. In *Proceedings of the 26th Annual International Conference on Machine Learning (ICML)*, pages 41–48, 2009.
- [27] Alex Graves, Marc G. Bellemare, Jacob Menick, Rémi Munos, and Koray Kavukcuoglu. Automated curriculum learning for neural networks. In *International Conference on Machine Learning (ICML)*, pages 1311–1320, 2017.
- [28] Tal Schuster, Adam Fisch, Jai Gupta, Mostafa Dehghani, Dara Bahri, Vinh Q. Tran, Yi Tay, and Donald Metzler. Confident adaptive language modeling. In *Advances in Neural Information Processing Systems*, 2022.
- [29] Yaniv Leviathan, Matan Kalman, and Yossi Matias. Fast inference from transformers via speculative decoding. In *International Conference on Machine Learning (ICML)*, pages 19274–19286, 2023.
- [30] Charlie Chen, Sebastian Borgeaud, Geoffrey Irving, Jean-Baptiste Lespiau, Laurent Sifre, and John Jumper. Accelerating large language model decoding with speculative sampling. *arXiv preprint arXiv:2302.01318*, 2023.
- [31] Shuyan Zhou, Frank F. Xu, Hao Zhu, Xuhui Zhou, Robert Lo, Abishek Sridhar, Xianyi Cheng, Tianyue Ou, Yonatan Bisk, Daniel Fried, Uri Alon, and Graham Neubig. Webarena: A realistic web environment for building autonomous agents. In *International Conference on Learning Representations (ICLR)*, 2024.
- [32] Reiichiro Nakano, Jacob Hilton, Suchir Balaji, Jeff Wu, Long Ouyang, Christina Kim, Christopher Hesse, Shantanu Jain, Vineet Kosaraju, William Saunders, et al. Webgpt: Browser-assisted question-answering with human feedback. *arXiv preprint arXiv:2112.09332*, 2021.
- [33] Shunyu Yao, Jeffrey Zhao, Dian Yu, Nan Du, Izhak Shafran, Karthik Narasimhan, and Yuan Cao. React: Synergizing reasoning and acting in language models. In *International Conference on Learning Representations (ICLR)*, 2023.
- [34] Noah Shinn, Federico Cassano, Edward Berman, Ashwin Gopinath, Karthik Narasimhan, and Shunyu Yao. Reflexion: Language agents with verbal reinforcement learning. In *Advances in Neural Information Processing Systems*, 2023.
- [35] Aman Madaan, Niket Tandon, Prakhar Gupta, Skyler Hallinan, Luyu Gao, Sarah Wiegrefe, Uri Alon, Nouha Dziri, Shrimai Prabhunoye, Yiming Yang, et al. Self-refine: Iterative refinement with self-feedback. In *Advances in Neural Information Processing Systems*, 2023.

- [36] Shunyu Yao, Dian Yu, Jeffrey Zhao, Izhak Shafran, Thomas L. Griffiths, Yuan Cao, and Karthik Narasimhan. Tree of thoughts: Deliberate problem solving with large language models. In *Advances in Neural Information Processing Systems*, 2023.
- [37] Timo Schick, Jane Dwivedi-Yu, Roberto Dessì, Roberta Raileanu, Maria Lomeli, Eric Hambro, Luke Zettlemoyer, Nicola Cancedda, and Thomas Scialom. Toolformer: Language models can teach themselves to use tools. In *Advances in Neural Information Processing Systems*, 2023.
- [38] Yujia Qin, Shihao Liang, Yining Ye, Kunlun Zhu, Lan Yan, Yaxi Lu, Yankai Lin, Xin Cong, Xiangru Tang, Bill Qian, et al. Toolllm: Facilitating large language models to master 16000+ real-world apis. In *International Conference on Learning Representations (ICLR)*, 2024.
- [39] Guanzhi Wang, Yuqi Xie, Yunfan Jiang, Ajay Mandlekar, Chaowei Xiao, Yuke Zhu, Linxi Fan, and Anima Anandkumar. Voyager: An open-ended embodied agent with large language models. *Transactions on Machine Learning Research*, 2024.
- [40] Xuezhi Wang, Jason Wei, Dale Schuurmans, Quoc Le, Ed Chi, Sharan Narang, Aakanksha Chowdhery, and Denny Zhou. Self-consistency improves chain of thought reasoning in language models. In *International Conference on Learning Representations (ICLR)*, 2023.
- [41] Jason Wei, Xuezhi Wang, Dale Schuurmans, Maarten Bosma, Brian Ichter, Fei Xia, Ed Chi, Quoc V. Le, and Denny Zhou. Chain-of-thought prompting elicits reasoning in large language models. In *Advances in Neural Information Processing Systems*, 2022.
- [42] Xuezhi Wang, Jason Wei, Dale Schuurmans, Quoc Le, Ed Chi, and Denny Zhou. Rationale-augmented ensembles in language models. *arXiv preprint arXiv:2207.00747*, 2022.
- [43] Hunter Lightman, Vineet Kosaraju, Yura Burda, Harrison Edwards, Bowen Baker, Teddy Lee, Jan Leike, John Schulman, Ilya Sutskever, and Karl Cobbe. Let’s verify step by step. In *International Conference on Learning Representations (ICLR)*, 2024.
- [44] Karl Cobbe, Vineet Kosaraju, Mohammad Bavarian, Mark Chen, Heewoo Jun, Lukasz Kaiser, Matthias Plappert, Jerry Tworek, Jacob Hilton, Reiichiro Nakano, et al. Training verifiers to solve math word problems. *arXiv preprint arXiv:2110.14168*, 2021.
- [45] Mark Chen, Jerry Tworek, Heewoo Jun, Qiming Yuan, Henrique Ponde de Oliveira Pinto, Jared Kaplan, Harri Edwards, Yuri Burda, Nicholas Joseph, Greg Brockman, et al. Evaluating large language models trained on code. *arXiv preprint arXiv:2107.03374*, 2021.
- [46] Eric Zelikman, Yuhuai Wu, Jesse Mu, and Noah D. Goodman. Star: Bootstrapping reasoning with reasoning. In *Advances in Neural Information Processing Systems*, 2022.
- [47] Caglar Gulcehre, Tom Le Paine, Srivatsan Srinivasan, Ksenia Konyushkova, Lotte Weerts, Abhishek Sharma, Aditya Siddhant, Alex Ahern, Miaosen Wang, Chenjie Gu, et al. Reinforced self-training (rest) for language modeling. *arXiv preprint arXiv:2308.08998*, 2023.
- [48] Avi Singh, John D. Co-Reyes, Rishabh Agarwal, Ankesh Anand, Piyush Patil, Xavier Garcia, Peter J. Liu, James Harrison, Jaehoon Lee, Kelvin Xu, et al. Beyond human data: Scaling self-training for problem-solving with language models. *Transactions on Machine Learning Research*, 2024.
- [49] Edward J. Hu, Yelong Shen, Phillip Wallis, Zeyuan Allen-Zhu, Yanzhi Li, Shean Wang, Lu Wang, and Weizhu Chen. Lora: Low-rank adaptation of large language models. In *International Conference on Learning Representations (ICLR)*, 2022.
- [50] Tim Dettmers, Artidoro Pagnoni, Ari Holtzman, and Luke Zettlemoyer. Qlora: Efficient finetuning of quantized llms. In *Advances in Neural Information Processing Systems*, 2023.
- [51] Woosuk Kwon, Zhuohan Li, Siyuan Zhuang, Ying Sheng, Lianmin Zheng, Cody Hao Yu, Joseph E. Gonzalez, Hao Zhang, and Ion Stoica. Efficient memory management for large language model serving with pagedattention. In *Proceedings of the 29th Symposium on Operating Systems Principles (SOSP)*, pages 611–626, 2023.
- [52] Tri Dao, Daniel Y. Fu, Stefano Ermon, Atri Rudra, and Christopher Ré. Flashattention: Fast and memory-efficient exact attention with io-awareness. In *Advances in Neural Information Processing Systems*, 2022.
- [53] Tri Dao. Flashattention-2: Faster attention with better parallelism and work partitioning. In *International Conference on Learning Representations (ICLR)*, 2024.

- [54] Tianle Cai, Yuhong Li, Zhengyang Geng, Hongwu Peng, Jason D. Lee, Deming Chen, and Tri Dao. Medusa: Simple llm inference acceleration framework with multiple decoding heads. In *International Conference on Machine Learning (ICML)*, 2024.
- [55] Tom B. Brown, Benjamin Mann, Nick Ryder, Melanie Subbiah, Jared Kaplan, Prafulla Dhariwal, Arvind Neelakantan, Pranav Shyam, Girish Sastry, Amanda Askell, et al. Language models are few-shot learners. In *Advances in Neural Information Processing Systems*, 2020.
- [56] Hugo Touvron, Louis Martin, Kevin Stone, Peter Albert, Amjad Almahairi, Yasmine Babaei, Nikolay Bashlykov, Soumya Batra, Prajjwal Bhargava, Shruti Bhosale, et al. Llama 2: Open foundation and fine-tuned chat models. *arXiv preprint arXiv:2307.09288*, 2023.
- [57] Thomas Wolf, Lysandre Debut, Victor Sanh, Julien Chaumond, Clement Delangue, Anthony Moi, Pierric Cistac, Tim Rault, Rémi Louf, Morgan Funtowicz, et al. Transformers: State-of-the-art natural language processing. In *Proceedings of the 2020 Conference on Empirical Methods in Natural Language Processing: System Demonstrations*, pages 38–45, 2020.

A Related work

Group-relative policy optimisation and its variants. GRPO [1, 2] replaces the learned value baseline of TRPO [15] / PPO [4] with the empirical mean of G rollouts of the same prompt; both descend from REINFORCE-style policy gradients [10, 16]. Several follow-up variants modify the advantage computation: RLOO [17] uses a leave-one-out estimator, ReMax [18] uses the maximum reward as the baseline, Dr.GRPO [19] removes the σ_r normalisation, and REINFORCE++ [20] adds token-level normalisation. None of these addresses the zero-variance group problem directly: when all G rewards are equal, any baseline based on the group itself yields zero advantage. They change the gradient magnitude on non-zero-variance groups but leave the wasted rollout cost on zero-variance groups untouched. The broader RLHF lineage [21, 22, 3], including DPO [23], Constitutional AI [24] and RLAI [25], shares the policy-gradient backbone but optimises against learned reward or preference models rather than environment-grounded rewards.

Filtering convergent groups: prompt-level and in-rollout. DAPO [8] drops zero-variance groups from the gradient batch after the rollouts have already finished, replacing them with new prompts to keep the batch full; exact but post-hoc. GRESO [9] predicts which prompts will be zero-variance before any rollout begins, using cross-epoch reward consistency on mathematical reasoning benchmarks. Both decide at the prompt level and are orthogonal to a mid-rollout decision. Curriculum-learning approaches [26, 27] also reweight prompts at the prompt level, by difficulty rather than by predicted variance. We are not aware of prior work that uses intermediate rollout state to predict zero-variance groups in GRPO. The closest single-trajectory analogues are early-exit inference: CALM [28] terminates a single generation when its per-token confidence saturates, and speculative decoding [29, 30] verifies a fast draft model against the target. These act on one trajectory; our setting requires a decision over a group of G trajectories using their disagreement as the signal.

LLM agents and agent RL benchmarks. ALFWorld [5], WebShop [6], WebArena [31], and AgentBench [7] are standard testbeds for LLM agent behaviour, with WebGPT [32] an early instance of agent RL on browser tasks. They share a structural property that mathematical reasoning benchmarks lack: every rollout is a multi-turn trajectory through an observable state space, so the shape of an in-progress group can be inspected at any intermediate step. ReAct [33] interleaves reasoning with action, Reflexion [34] and Self-Refine [35] add verbal self-critique, Tree-of-Thoughts [36] explores multiple reasoning branches, and Toolformer [37] / ToolLLM [38] expand the action space with API calls. Voyager [39] embeds an LLM agent in an open-ended environment with skill acquisition. These contributions design *what* the policy does inside a rollout; ours is about *when to stop* the rollout.

Multi-sample inference and training efficiency. The $G \times$ multi-sample structure also appears at inference time: self-consistency [40] takes a majority vote over G chain-of-thought [41] rollouts, rationale-augmented ensembles [42] aggregate weighted samples, best-of- N sampling with a verifier or reward model picks the best of N candidates [43, 44], and pass@ k [45] is the standard G -sample capacity-evaluation metric. The same divergence signal applies to these settings. A complementary line of work reuses trajectories for self-training rather than discarding them: STaR [46], ReST [47] and *Beyond human data* [48] iterate on model-generated solutions filtered by reward, which *exploits* successful rollouts where our gate *cuts* saturated ones. Orthogonal lines of work reduce per-token cost via parameter-efficient fine-tuning (LoRA [49], QLoRA [50]) and inference-system optimisations (PagedAttention [51], FlashAttention [52, 53], Medusa [54]); our gate reduces the *number* of steps generated rather than the cost of each step. Throughout we use Qwen2.5-7B-Instruct [11] as the base policy, in line with current open-base-model practice [55, 56].

B Full mid-rollout signal definitions

The body (§3.2) defines d_K and points here for the other six in-group divergence signals we considered. Each is a scalar in $[0, 1]$ computed from the G partial trajectories at step K , with 0 meaning the trajectories are identical at that point.

- **prefix_edit_distance_mean** (d_K). The body signal: mean over $\binom{G}{2}$ pairs of the Levenshtein edit distance between $a_{i,1:K}$ and $a_{j,1:K}$, divided by the longer length.

- **action_bigram_jaccard_mean.** For each pair of trajectories, take the set of consecutive action pairs (action bigrams) in each trajectory’s first K steps, compute the Jaccard overlap of the two sets, and report 1 minus that overlap. Average over all pairs. Like d_K this is 0 when the trajectories use the same action transitions and grows as they diverge.
- **unique_prefix_ratio.** Number of distinct trajectories among $a_{i,1:K}$, divided by G . The minimum $1/G$ means all G trajectories share the same first- K sequence; the maximum 1 means every trajectory is different. **unique_action_ratio** is the same quantity computed on the single action $a_{i,K}$ at step K rather than on the full prefix.
- **action_entropy.** Shannon entropy of the empirical distribution of $\{a_{i,K}\}$ across the G trajectories at step K .
- **obs_unique_ratio.** Same as **unique_action_ratio** but on the environment observation $o_{i,K}$ rather than the action; a proxy for whether the trajectories have reached the same world state.
- **termination_fraction** (τ_K). Fraction of the G trajectories that have already finished (either succeeded or failed) by step K . $\tau_K=0$ means no trajectory is done, $\tau_K=1$ means all G are done. Note this signal is not itself in $[0, 1]$ as a divergence measure (it is unimodal in the group label), and we include it only as a complementary candidate for the OR-rule extension in App. E.9.

The full 7×4 side-by-side comparison (Spearman ρ and AUROC for each metric at $K \in \{5, 10, 15, 20\}$) is in App. E.3.

C Implementation details

C.1 How the gate is enforced inside a rollout

The rollout loop generates the G trajectories of a group one environment step at a time. After the K -th environment step we pause the loop and compute the in-group divergence d_K on the partial trajectories produced so far. If d_K falls below the threshold d_L , every trajectory in the group is recorded as terminated at step K with whatever reward it has accumulated by then, and the rollout loop exits early for that group. The remaining $T_{\max} - K$ steps are not generated. **The accumulated step- K rewards are kept on the trajectory records only for logging and visualization** (e.g. the training-reward panel of Fig. 4 subtracts cut groups precisely because their truncated reward of 0 is not a real outcome); **the cut group itself is dropped from the GRPO advantage and loss computation entirely** (§3.2, line ‘if is_cut: continue’ in the released code), so these truncated rewards never enter the gradient. When multiple rollouts run in parallel on different GPUs, each applies the gate independently and the wall-clock saving on the full set of groups is the sum of per-group savings. No model parameters are changed during this rollout phase; the gate only affects how much of each group’s trajectories is generated.

C.2 Teacher-forcing GRPO loss in agent setting

After rollout, each trajectory τ is a token sequence [prompt, $o_1, a_1, o_2, a_2, \dots, o_T, a_T$] where o_t is the environment observation at step t and a_t is the model’s response. Only a_t tokens are produced by π_θ ; o_t tokens are environment-injected. Computing the policy-gradient loss requires $\log p_\theta(a_t \mid \text{prefix})$ at every action-token position.

We compute this with a single teacher-forcing forward pass: the entire token sequence is fed into the policy model with a causal attention mask, which returns logits at every position. The logit at position $t - 1$ predicts the token at position t ; we extract log-softmax values at each *action-token* position only — observation-token positions are masked out, since the policy did not produce them. The trajectory log-likelihood is $\log p_\theta(\tau) = \sum_{t \in \mathcal{A}} \log p_\theta(\tau_t \mid \tau_{<t})$ where \mathcal{A} is the set of action-token positions, and the policy-gradient loss is $\mathcal{L} = -A \cdot \log p_\theta(\tau)$.

The action-token mask is constructed at rollout time and stored alongside the token IDs. Without it, the loss would also penalise θ for “predicting” the environment’s observations, which is both incorrect (those tokens were not generated by θ) and empirically destabilising (large gradient-norm spikes when the environment emits unexpected text).

C.3 Reloading the policy between iterations

The on-policy training run in Tier 3 alternates between sampling rollouts and updating the policy. After each gradient update, the trained LoRA adapter weights are written to disk and then loaded back into the inference engine before the next iteration’s rollouts begin. The base model itself stays resident in GPU memory and is not reloaded; only the small LoRA delta is swapped. The total round-trip cost is on the order of one second per iteration at LoRA rank 16, which is negligible compared to the time spent generating the iteration’s rollouts.

C.4 Hyperparameters

Table 6 lists the hyperparameters used in each of the three integration tiers. The same gate setting $(K, d_L) = (10, 0.12)$ is used in all three tiers, chosen on the offline buffer in §3.5 and not retuned for the online runs. Tier 1 has no training so the LoRA and optimiser hyperparameters do not apply. Tier 2 uses a smaller LoRA rank ($r = 8$, two target modules) because the buffer is fixed and the optimisation is short (20 steps); Tier 3 uses a larger LoRA rank ($r = 16$, seven target modules) because the policy must continue to learn over 60 on-policy iterations. The sampling temperature during rollout is 0.7 in all tiers, which keeps the G trajectories of a group meaningfully different from each other; held-out evaluation in Tier 3 uses greedy decoding (temperature 0) so each test task is decoded once and the outcome is deterministic.

Table 6: Hyperparameters across the three integration tiers.

	Tier 1 (rollout-only)	Tier 2 (off-policy)	Tier 3 (on-policy)
prompts	100 (baseline & gated, same seed)	100 (replay buffer)	60×10 resampled
gradient steps	0	20	60
groups per step	—	4	10
action steps used per traj.	—	8 (sampled)	all
LoRA rank / α	—	8 / 16	16 / 32
LoRA targets	—	q, v	q, k, v, o, MLP
optimizer	—	AdamW	AdamW
learning rate	—	5×10^{-5}	5×10^{-5}
sample temp. (rollout)	0.7	0.7	0.7
sample temp. (eval)	—	—	0 (greedy)
T_{\max}	30	30	30
G	8	8	8
gate (K, d_L)	(10, 0.12)	(10, 0.12)	(10, 0.12)
random seed	42	42	{7, 13, 23, 42}

C.5 Setting the precision floor

The 0.80 precision floor is set so that the worst-case impact on the un-gated GRPO advantage L^2 -norm is bounded by a tolerable fraction η . Concretely, if the gate’s precision is p , then the fraction of *useful* groups (non-zero-variance) it incorrectly cuts is $(1-p) \cdot |\text{cut}|/|\text{nonzero-var}|$. For the main single-axis gate at $d_L = 0.12$: $|\text{cut}| = 21$, $|\text{nonzero-var}| = 61$, $p = 0.81 \rightarrow$ fraction lost $\approx 21 \cdot 0.19/61 \approx 6.5\%$ of useful groups. The empirical gradient- L^2 loss (3.3%, §3.5) is even smaller because the falsely-cut groups had below-average $|A_i|$. To target a worst-case $\eta = 10\%$ gradient-norm loss with our group composition, the precision floor is $1 - \eta \cdot |\text{nonzero-var}|/|\text{cut}| \approx 1 - 0.10 \cdot 61/21 \approx 0.71$, well below 0.80; the floor is thus a conservative choice.

C.6 Hardware and timing

All experiments use NVIDIA RTX 6000 Ada (48 GB) GPUs. Tier 1 runs the 100 tasks across 4 GPUs in parallel. Tiers 2 and 3 each use two GPUs, one dedicated to sampling rollouts and one dedicated to running the gradient update. Each on-policy training run (baseline or gated) takes 4.5 to 4.8 hours. Total compute used for the paper is approximately 30 GPU-hours. Inference uses vLLM [51] and gradient updates use the Hugging Face Transformers [57] and PEFT/LoRA [49] stacks.

D Extended discussion

D.1 Mechanistic explanation of the held-out gain

The held-out improvement we report in Tier 3 (§4.3) has two candidate explanations. The first is that the gate changes the *set* of training prompts in a way that biases generalisation. The second is that the gate changes the *magnitude* of each gradient step without changing its expectation. We have direct evidence for the second and against the first.

Evidence for the gradient-magnitude explanation. The dilution analysis in §4.4 predicts a gradient amplification factor of about 1.20 at the cut rate we observe. The measured factor is 1.16 ± 0.07 across the 4 seeds (Table 5), close to the prediction. The mechanism is mechanical and predictable: removing zero-advantage trajectories from the batch shrinks the denominator of the loss mean while leaving the numerator unchanged.

Evidence against the prompt-distribution explanation. When the gate cuts a group, that group is dropped from the gradient batch but the prompt is not re-sampled. The next training iteration draws a fresh batch of 10 prompts uniformly at random from the same training pool. The gate therefore does not bias the prompt distribution, and any distribution-shift explanation of the held-out gain is ruled out by construction.

Practical implication. A practitioner who does not want to use the gate could approximate the held-out gain by raising the learning rate by about $1.16\times$ in the baseline. This approximation is crude, however, because the zero-advantage fraction varies between iterations (we see 25% to 70% across the 60 iterations of our run). The gate scales the effective learning rate dynamically per iteration, which a fixed learning-rate increase cannot match.

D.2 Future directions

Environment-grounded progress signals for high- d_K all-failure groups. The gate catches the low- d_K end of the all-fail cluster (10/25 in our buffer; §3.4) but cannot reach the high- d_K majority because their early-action prefixes overlap with mixed-outcome groups in the same d_K region. Detecting them would require a signal beyond what the partial trajectories themselves provide: for example, an intermediate progress proxy from the environment (“object picked up”, “sub-goal reached”) that distinguishes a stuck rollout from one that is still exploring. ALFWorld and most agent benchmarks expose such proxies, but using them is outside the scope of this paper.

Per-group choice of the gate evaluation step. We use a fixed $K = 10$ throughout. Some groups become unambiguously zero-variance much earlier (the trajectories collide on identical prefixes by $K = 5$); others are not separable until $K = 15$. A model that predicts the optimal K for each group from a few early steps of the rollout could recover further compute.

Composition with DAPO and GRESO. Our gate is orthogonal to both filters. GRESO can skip a prompt before any rollout begins, our gate can stop a group’s rollout partway through, and DAPO can drop a group from the gradient batch after the rollout has finished. The three operate at three distinct stages of the training pipeline and compose naturally. A natural follow-up is to measure the combined saving end-to-end.

E Detailed experimental results

E.1 Calibration against random-cut and oracle gates

We compare our gate against two reference policies that are not prior work, but do bracket what any cut policy operating at the same cut rate can do.

The first is a **random-cut** policy that fires on 20% of groups uniformly at random, matching our gate’s overall cut rate. This policy destroys 12.4% of the GRPO advantage signal (measured as the L^2 -norm of the advantage vector before vs after cutting), because cutting a non-zero-variance group throws away real gradient information. Our gate, by contrast, preserves 96.7% of the advantage

signal at the same cut rate, confirming that it is selecting groups in an information-aware way rather than dropping rollouts blindly.

The second is an **oracle** policy that has access to the ground-truth zero-variance label and cuts every zero-variance group at step $K = 10$. The oracle sets the upper bound on what any gate of this form can save: 23.1% of total rollout step-tokens (raw, using actual rollout step counts). Our gate recovers 11.3% on the same formula, $\sim 49\%$ of the oracle’s ceiling. The remaining gap to the oracle is the high- d_K tail of the zero-variance groups (mostly all-fail): their early-action prefixes look the same as those of mixed-outcome groups, so no threshold on prefix divergence alone can separate them. Closing this gap would require a different signal, not a better threshold.

E.2 Bootstrap confidence intervals on the headline savings

The Tier 1 A/B run (§4.1, Table 3) is the direct measurement of the gate’s wall-clock effect: the gated arm finishes 13.25% faster than the matched baseline on the same 100 ALFWorld tasks. To check that this saving is robust to the particular set of 100 tasks we drew, we resample the 100 task-level wall-clock differences with replacement 1,000 times and recompute the percentage saving each time. The bootstrap 95% confidence interval is [7.55, 19.12]%; the interval excludes zero.

The offline analysis of §3.5 makes a parallel prediction. Counting step-tokens directly in the original 100-task buffer, the gate at $d_L = 0.12$ would have recovered 11.3% of total step-tokens (17 true-positive groups times the $T_{\max} - K = 20$ post- K steps each, divided by the total 100×30 step budget). Bootstrapping that step-token saving over the same task resampling gives a 95% confidence interval of [8.0, 18.0]%. The Tier 1 wall-clock measurement falls inside this predicted band, confirming that the offline step-token saving translates into actual GPU wall-clock once the gate is enforced online.

E.3 Full correlation table

Table 7: Spearman ρ of each (metric, K) cell against group reward variance σ_r^2 , $N = 100$, $G = 8$. Cells in **bold** exceed the pre-registered threshold $|\rho| \geq 0.40$. Termination fraction has near-zero monotone correlation by design (U-shape against label).

metric	$K = 5$	$K = 10$	$K = 15$	$K = 20$
prefix_edit_distance_mean (d_K)	0.246	0.374	0.419	0.418
action_bigram_jaccard_mean	0.293	0.407	0.406	0.389
unique_prefix_ratio	0.320	0.398	0.307	0.208
unique_action_ratio	0.314	0.379	0.272	0.167
action_entropy	0.292	0.369	0.255	0.161
obs_unique_ratio	0.251	0.397	0.307	0.093
termination_fraction (τ_K)	-0.188	-0.059	0.110	0.235

E.4 False-positive case analysis

At $d_L = 0.12$ the gate flags 4 groups whose final rewards turn out not to be zero-variance: the gate predicted convergence but the group ended mixed. All 4 are `pick_and_place_simple` tasks in which the model emits the same fixed drawer-by-drawer search prefix in every trajectory of the group, so the gate sees low divergence at $K = 10$ and fires. The trajectories then diverge *after* step $K = 10$ depending on whether the queried object happens to be in one of the first few drawers searched: some trajectories find it and succeed, others do not, so the group’s final rewards are mixed even though its first 10 actions agree. This points to a specific failure mode of an action-prefix divergence signal: the signal cannot detect future divergence in the *environment-state* branching after the prefix has been fixed.

E.5 Per-task-type correlation breakdown

Table 8 reports the gate signal for each of the six ALFWorld task types, in two forms: the global metric d_{10} that the gate actually uses, and the post-hoc best (*metric*, K) pair per type. The global d_{10} generalises unevenly: it is excellent on `look_at_obj_in_light`, `pick_heat`, and `pick_two_obj`

(AUROC ≥ 0.91) but degrades on `pick_and_place_simple`, `pick_clean`, and `pick_cool` (AUROC 0.48–0.62). Allowing the $(metric, K)$ pair to be tuned per type recovers the worst three to AUROC 0.71–0.86, with `termination_fraction` at $K = 15$ – 20 being the best signal in the harder pick-cool / pick-clean tasks. The two task types where the per-type best is AUROC 1.00 have only $n_{zv} = 1$ – 2 positives, so those cells are essentially single-observation; they should be read as “the gate did not fail” rather than “perfect”.

Table 8: Per-task-type AUROC for the (binary) zero-variance vs non-zero-variance classification at the published gate’s evaluation step $K = 10$. **Global d_{10} AUROC** is the metric the gate actually uses; **Best AUROC** is the maximum over $(metric, K)$ tuned per task type, with the winning pair in parentheses. n = groups in that type; n_{zv} = zero-variance groups (the positive class).

Task type	n	n_{zv}	Global d_{10} AUROC	Best $(metric, K)$	Best AUROC
<code>pick_and_place_simple</code>	24	13	0.62	(<code>unique_action_ratio</code> , 15)	0.86
<code>pick_two_obj_and_place</code>	20	13	0.91	(<code>termination_fraction</code> , 20)	0.86
<code>pick_cool_then_place</code>	19	5	0.48	(<code>termination_fraction</code> , 20)	0.82
<code>pick_clean_then_place</code>	18	5	0.56	(<code>termination_fraction</code> , 15)	0.71
<code>pick_heat_then_place</code>	11	1	1.00*	(<code>action_entropy</code> , 10)	1.00*
<code>look_at_obj_in_light</code>	8	2	1.00*	(<code>unique_prefix_ratio</code> , 15)	1.00*
median	—	—	0.76	—	0.86

* $n_{zv} \leq 2$, single-observation regime.

E.6 $G = 8$ vs $G = 16$ robustness panel

The whole paper uses a group size of $G = 8$. To check that our findings still hold at a larger group size, we re-collected the $N = 100$ ALFWorld rollouts with $G = 16$ trajectories per prompt and recomputed the divergence measures and correlations.

Two things stay essentially unchanged. The group-label composition is similar: 25 all-fail, 61 mixed, 14 all-succeed at $G = 8$ vs 25 all-fail, 62 mixed, 13 all-succeed at $G = 16$ (39 vs 38 zero-variance groups out of 100). The shape of the correlation curve in K is also similar (Figure 5): the divergence-variance correlation rises from $K = 5$, peaks around $K = 10$ – 15 , and is roughly flat or slightly decreasing afterwards, in both group sizes.

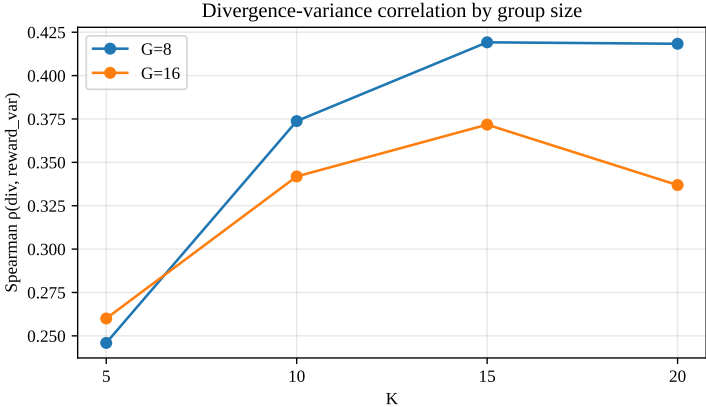


Figure 5: Spearman ρ between mid-rollout divergence d_K and final reward variance σ_r^2 , plotted as a function of the gate evaluation step K , for two group sizes ($G = 8$ and $G = 16$) on the same 100 ALFWorld tasks. The shape of the curve is the same in both group sizes; the peak value is slightly lower at $G = 16$ (0.37 vs 0.42), which we explain in the text.

The peak correlation is slightly lower at $G = 16$ ($\rho = 0.37$ at $K = 15$) than at $G = 8$ ($\rho = 0.42$). The reason is mechanical: at $G = 8$ a converged group (whether heading to a common success or stuck in a common failure) often has all eight trajectories choose the same first K actions, giving $d_K \approx 0$ and a clear separation from non-zero-variance groups; at $G = 16$ it is more common that at least one of

the sixteen trajectories takes a slightly different first action, so d_K is no longer near zero even when the group ends up zero-variance. This thins the low- d_K zero-variance cluster (both all-succeed and all-fail) a little and reduces the rank correlation.

Threshold transfer is partial. Applying the single-axis gate ($K = 10, d_L = 0.12$) verbatim to the $G = 16$ data flags more groups but at lower precision, because with more samples per group it is more likely that a non-zero-variance group happens to share a low-divergence prefix by chance. Re-fitting the threshold on $G = 16$ at the same 0.80 precision floor moves the operating point to ($K = 15, d_L = 0.09$), with savings of about 7.0%, strictly lower than at $G = 8$ because each cut group at $K = 15$ recovers only $T_{\max} - K = 15$ remaining steps instead of 20. The gate transfers across group sizes, but its threshold should be retuned at each G .

E.7 Off-policy training per-step trace

In Tier 2 each training step samples 4 groups from the buffer. For every trajectory in those groups (at most $4 \times G = 32$ trajectories per step), the trainer samples up to 8 action positions and computes the policy-gradient loss at each one. A “training item” in the figure below is one such (trajectory, action position) pair, so the maximum number of items per step is $4 \times 8 \times 8 = 128$. In the gated arm a cut group contributes zero items, so each cut removes up to $8 \times 8 = 64$ items.

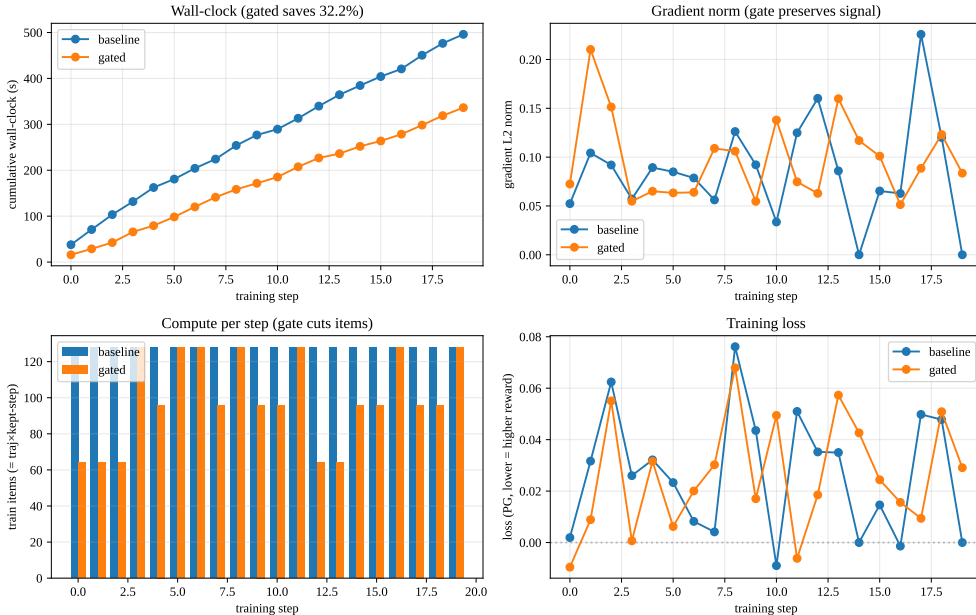


Figure 6: 20-step off-policy GRPO training A/B on Qwen2.5-7B + LoRA. *Top left*: cumulative wall-clock; the gated arm finishes 32.2% faster end-to-end. *Top right*: per-step gradient L^2 -norm; the gated arm runs at about 114% of baseline. *Bottom left*: number of training items per step (one item = one trajectory \times one action position; max 128 as explained above). The baseline arm always uses the maximum 128 items because no group is cut. The gated arm drops to between 64 and 128 items per step depending on how many groups the gate cut at that step. *Bottom right*: per-step training loss. Both arms sit in the same noisy band around zero. This is expected: by definition the GRPO advantages within a group sum to zero, so the population loss for the population gradient estimator is zero up to noise. A loss near zero in this plot does not mean the policy stopped learning; held-out evaluation in Tier 3 is the metric that captures policy quality.

E.8 On-policy training per-iter trace and held-out trajectory

In Tier 3, every 10 iterations we pause training and run greedy decoding on 50 held-out ALFWorld tasks (§4.3). Table 9 shows the resulting success rate at each of the 7 evaluation points (iters 0, 10, 20, ..., 60), averaged over the 4 random seeds we ran. At iter 0 no training has happened

yet, so the gated and baseline arms share the same policy by construction and therefore evaluate identically per seed (the across-seed std is non-zero because the held-out task set is seeded from the run’s random seed). The held-out gap between the two arms is non-monotonic across iterations: gated is slightly behind at iters 20–30 and slightly ahead from iter 40 onward. The +2.5 pp mean gap we report at iter 60 in the main text is one point on this noisy trajectory.

Table 9: Held-out success rate across the 60 on-policy iterations, averaged over the 4 seeds. Δ is the per-seed mean of (gated – baseline). At iter 0, gated and baseline are the same policy (same random seed), so per-seed they coincide and $\Delta = 0$ exactly. Across-seed standard deviations are reported in Figure 4 (shaded bands) and Table 5 (iter 0 and iter 60).

iter	0	10	20	30	40	50	60
baseline	39.5%	38.5%	39.5%	40.5%	39.0%	37.0%	41.5%
gated	39.5%	39.5%	38.0%	37.5%	43.5%	40.0%	44.0%
Δ	0	+1.0	-1.5	-3.0	+4.5	+3.0	+2.5

Per-iter gate firing pattern. The per-iter cut count is highly variable, ranging from 0 to 6 groups (out of the 10 in each iteration) depending on the difficulty of the iteration’s sampled prompts. Across the 4 seeds and 60 iterations the gate fires on a mean of 106 ± 18 groups out of 600 total (17.7% cut rate; per-seed totals 88, 94, 119, 124 for seeds 13, 7, 23, 42). The mean baseline zero-variance rate over the same iters is 40.6%, and the gate’s per-iter recall on the on-policy zero-variance ground truth averages $\sim 37\%$, comparable to the $17/39 \approx 44\%$ recall on the offline buffer (Table 1), indicating the gate’s selectivity is preserved under the on-policy distribution shift.

Has the policy converged? The training reward variance does not collapse over the 60 iterations in either arm, so neither policy has reached a fixed point within the compute budget we used. The wall-clock saving is a per-iteration percentage and should therefore stay roughly constant ($\sim 10.7\%$) regardless of how many iterations we run. The held-out gap between the gated and baseline arms, however, could either widen with more iterations (if the gradient-amplification effect from §4.4 keeps the gated arm slightly ahead at every step) or shrink to zero (if both arms eventually reach the same converged policy). The $n = 4$ seeds and 60 iterations we run cannot distinguish these two scenarios; longer training runs are left to future work.

E.9 The OR-rule extension: optional termination-fraction backup

The main paper uses a one-parameter single-axis gate $\text{CUT}_{K,d_L} : \text{cut iff } d_K < d_L$ (§3.2). We document here a two-parameter *OR-rule* extension we explored:

$$\text{CUT}_{K,d_L,\tau_H}^\vee : d_K < d_L \vee \tau_K \geq \tau_H, \quad (3)$$

which adds a backup clause that triggers when most of the group has already terminated. The motivation is the U-shape between τ_K and the group label (Table 10 below): all-success groups concentrate at high τ_K and low d_K ; high τ_K contains a few extra all-success groups whose trajectories arrived at the goal via slightly different short prefixes that the d -threshold misses.

Table 10: Median of d_K and τ_K at $K = 15$ stratified by group label, $G = 8$. The two zero-variance classes (all-fail, all-succeed) sit on *opposite* ends of τ_K , motivating the U-shape interpretation that originally led us to the OR-rule.

group label	n	median d_{15}	median τ_{15}	physical meaning
all_succeed	14	0.19	1.00	solved fast, all terminated
mixed	61	0.47	0.13	exploring different strategies
all_fail	25	0.26	0.00	nobody finishes, often lock-stepped

Quantitative effect of adding the τ backup. At $K = 10$, $\tau_H = 0.90$, $d_L = 0.12$, the OR-rule extension flags 23 groups (vs 21 for $d_K < 0.12$ alone) and hits all 2 extra groups as true positives, yielding precision 0.83 vs 0.81 and recall 0.49 vs 0.44. **However, the incremental rollout savings is exactly zero:** by step $K = 10$ those 2 extra groups have $\tau \geq 0.90$ — i.e., 7–8 of their $G = 8$

trajectories have *already* terminated, so “cutting” them at K saves nothing the early-termination mechanism didn’t already save (Table 12).

We therefore recommend the single-axis gate as the production default: simpler, less prone to overfitting on small validation sets ($N = 100$ here), and indistinguishable in rollout savings. The OR-rule is documented for completeness and would be the natural extension on environments where τ_K at moderate K is more discriminative than ALFWorld provides.

Trying to catch all-failure groups. The OR-rule above adds a backup clause for the all-success end of the U-shape ($\tau_K \geq 0.90$). The natural mirror, which would catch all-failure groups, is to add a backup clause for the low- τ end: $d_K < d_L \vee \tau_K \leq t_L$. We swept this rule across $d_L \in [0.02, 0.30]$, $t_L \in \{0, 0.05, 0.10, 0.15\}$, and $K \in \{5, 10, 15, 20\}$. *No operating point clears the 0.80 precision floor at any K .* The reason is geometric: in early rollout phases mixed groups also have $\tau_K \approx 0$ (some trajectories are still running, none has reached a terminal state yet), so any cut on low τ_K pulls many mixed groups in along with the all-failure ones it was meant to catch. This is the empirical evidence behind the “no operating point clears 0.80 precision” claim in the contributions section of the main paper.

E.10 OR-rule training A/B (seed 42, R3)

Before pivoting to the single-axis R1 gate, we ran the on-policy training A/B with the two-parameter OR-rule extension R3 (App. E.9) on seed 42. We report those numbers here for completeness:

Table 11: On-policy A/B with the OR-rule extension R3 ($d_K < 0.12 \vee \tau_K \geq 0.90$), seed 42, 60 iters. Setup otherwise matches Tier 3 in the main paper.

	baseline	gated (R3)	Δ
total wall-clock (s)	17,252	15,364	-10.94%
groups cut / total	0/600	96/600	cut rate 16.0%
zero-advantage items in batch	42.0%	25.7%	-16.3 pp
gradient L^2 -norm mean	0.123	0.181	+47%
held-out eval, iter 0/60	38.0%/38.0%	38.0%/46.0%	+8 pp
bootstrap 95% CI on Δ		[+2, +16] pp	CI excludes 0

On this single seed (seed 42), the OR-rule extension gives a +8 pp held-out improvement over its baseline. The single-axis gate on the same seed gives +2 pp, and across the four single-axis seeds we report in the main paper (seeds $\{7, 13, 23, 42\}$) the held-out improvement is $+2.5 \pm 3.4$ pp on average. The OR-rule’s larger improvement on this single seed is consistent with its larger dilution reduction: it cuts about 16.0% of groups (vs 17.7% for single-axis), and its zero-advantage-item rate drops by -16.3 pp (vs about -12 pp for single-axis), giving a larger gradient amplification ($1.47 \times$ vs $1.16 \pm 0.07 \times$).

We caution that this OR-rule run is on a single seed and that the OR-rule has two parameters tuned on the same $N = 100$ offline buffer, so the comparison overstates the OR-rule’s true held-out improvement relative to single-axis. Without OR-rule runs on additional seeds, we cannot say how much of the +8 pp vs +2.5 pp gap is the rule and how much is seed variance. We report the OR-rule numbers here for completeness and as an upper-bound reference for what the gate’s policy-improvement effect could look like under more aggressive cutting; we use the single-axis gate for all main-paper claims.

E.11 Strong-baseline comparison detail

DAPO-oracle (post-hoc only) saves 0% rollout compute by construction — DAPO drops zero-variance groups from the gradient batch but does not interrupt the rollout. In the off-policy training A/B (Tier 2, Sec. 4.2) DAPO-oracle would save the forward+backward of zero-variance groups, which translates to a training-phase saving (we measure 32.2% wall-clock there). **OURS R1 + DAPO** is the recommended combination for an end-to-end production trainer: cut early on the divergence signal, then drop any surviving zero-variance groups from the gradient batch.

Table 12: Strong-baseline arm comparison on the same $N = 100$ buffer; cut count, TP/FP composition, precision, rollout step-tokens saved, and GRPO advantage L^2 -norm preserved (ratio to no-gate). Random-cut at the same ~ 23 -cut budget destroys ~ 12 pp of L^2 because its FPs land on non-zero-variance groups whose advantages are real. Oracle (cut iff truly zero-variance) sets the upper bound at 23.1% saving; our single-axis gate $d_K < 0.12$ recovers 51% of that at 96.7% L^2 -preservation. DAPO-oracle and OURS+DAPO save the same rollout step-tokens as their pre-DAPO counterparts because DAPO is a post-rollout filter that drops groups from the gradient batch only; it changes the training-phase cost (App. E.7), not the rollout-phase cost. The single-axis $\tau_K \geq 0.90$ clause on its own saves zero rollout compute because the groups it fires on have already terminated by step K .

arm	cut	TP	FP	precision	rollout-saved (%)	L^2 -preserved (%)
no-gate	0	0	0	—	0.0	100.0
random-cut (matched 23)	23	9	14	0.39	13.3	87.6
oracle (cut iff zv)	39	39	0	1.00	23.1	100.0
DAPO-oracle (post-hoc filter only)	0	0	0	—	0.0	100.0
OURS R1 ($d_K < 0.12$)	21	17	4	0.81	11.3	96.7
single-axis $\tau_K \geq 0.90$ only	6	6	0	1.00	0.0	100.0
OR-rule extension R3 ($d \vee \tau$)	23	19	4	0.83	11.3	96.7
OURS R1 + DAPO	21	17	4	0.81	11.3	96.7

E.12 Mechanism evolution: zv-rate, dilution, and gate recall over training

The top-left panel of Figure 7 plots the per-iteration zero-variance rate in both arms, smoothed with a 5-iteration rolling average. The baseline rate fluctuates between 10% and 90% across iterations and drifts slowly downward (mean 42%), consistent with the policy gradually moving from all-fail-dominated zero-variance groups (more common early in training) toward more mixed-outcome groups as it learns to succeed on at least some of the G rollouts.

For the gated arm we compute the zero-variance rate over the *uncut* groups only. We exclude cut groups from this statistic because the gate stops their trajectories at step $K = 10$ before any reward has arrived in ALFWorld (most successes happen at step 15–25), so their recorded rewards are all zero and they would be miscounted as zero-variance even when their full rollout would have been mixed. With this correction, the gated zero-variance rate is 37.1% on average, modestly below baseline as expected: the gate has removed some genuinely zero-variance groups from the rollout distribution, leaving a slightly less zero-variance-heavy remainder.

The top-right panel anchors the gate’s recall on the on-policy distribution. The blue line is the baseline-arm ground-truth zero-variance rate (the gate had no effect on baseline rollouts); the orange line is the per-iteration cut rate in the gated arm. The gray band between them is the recall gap: ground-truth zero-variance groups that the gate did not cut. On average, the gate’s per-iteration recall against this ground truth is 34.8%, lower than the offline 0.49 we report in §3.5 because the on-policy rollout distribution differs from the offline buffer that the threshold was tuned on. The gate behaves conservatively under this shift, which is why its precision stays high.

E.13 Token-level dilution measurement

We estimate the zero-advantage dilution rate directly from the per-iteration training logs of the on-policy run. For each iteration we know how many groups were rolled out, how many ended up zero-variance, and how many were cut by the gate. With $G = 8$ trajectories per group and 10 groups per iteration, the un-gated baseline’s zero-advantage fraction averages about 42%, and the gated run’s zero-advantage fraction (from the zero-variance groups that survived the gate) averages about 26%. The ≈ 16 percentage-point reduction is what drives the gradient-norm amplification reported in §4.4.

F Prompt templates

ALFWorld system prompt. We use a ReAct-style prompt format. The system message describes the ALFWorld environment, lists the canonical action vocabulary, and provides one in-context example trajectory. The user message at each step contains the current observation, and the assistant is expected to emit text in the format “Thought: ... Action: <action>”. The action string

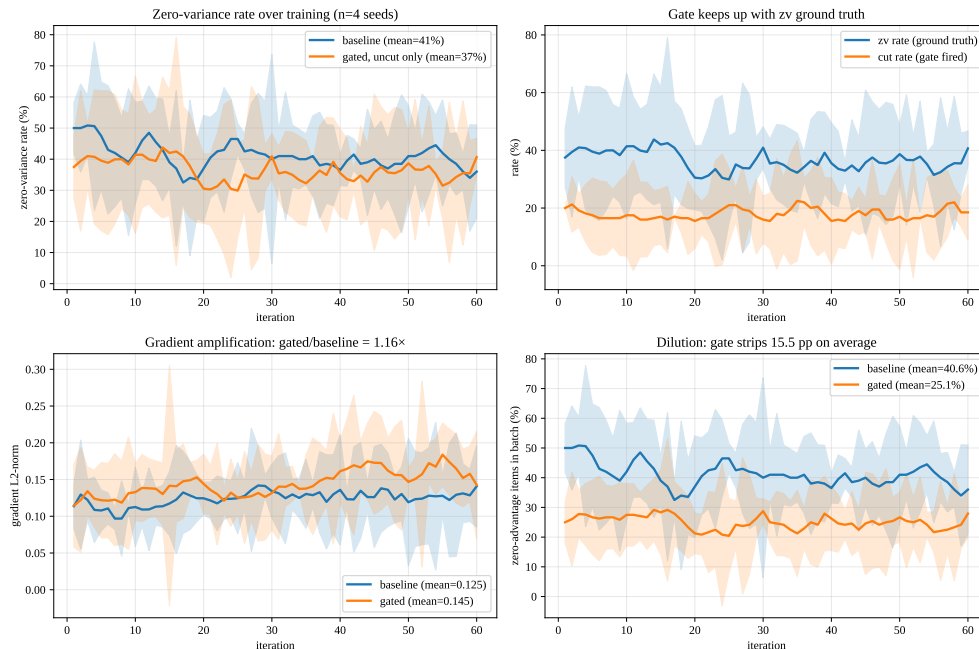


Figure 7: Mechanistic evolution across the 60-iteration on-policy GRPO training, averaged over $n = 4$ seeds $\{7, 13, 23, 42\}$; shaded bands are ± 1 std across seeds. *Top-left*: per-iter zv rate (5-iter rolling) drifts downward in the baseline as the policy learns; gated tracks closely on the uncut groups. *Top-right*: gate cut rate (orange) vs ground-truth zv rate (blue) per iter; per-iter recall averages 37.2%. *Bottom-left*: gradient L^2 norm — gated runs $1.16\times$ baseline on average (1.16 ± 0.07 across seeds), matching the dilution prediction (§4.4, Table 5). *Bottom-right*: zero-advantage-item rate in the train batch: baseline 40.6%, gated 25.1%, a -15.5 pp reduction which is the proximate mechanism for the held-out gain.

is parsed greedily; if it does not match the environment’s action grammar, the step is treated as a no-op and still counts towards T_{\max} .

Eval prompt. Held-out eval (Tier 3) uses the same prompt format but with sampling temperature $T = 0$ (greedy) and no gate. A task is counted as solved iff the environment returns $r = 1$ within $T_{\max} = 30$ steps.

G Broader impacts

The selective-rollout gate reduces the compute footprint of agent RL training by 11–32% on our benchmark, with no degradation in downstream policy quality — and in the on-policy setting, with a measurable improvement. The direct effect is to lower the energy and GPU-time cost of LLM agent training, which aligns with the broader goal of making such training accessible to research groups without hyperscale compute. We do not foresee novel dual-use risks beyond those already inherent to LLM agent RL: any compute-saving technique applied to capability research generally accelerates capability research, including capabilities that may have negative externalities (e.g. autonomous web agents executing harmful actions). The gate itself is agnostic to the reward function and does not introduce new incentives.